RSC Advances

PAPER

View Article Online
View Journal | View Issue



Cite this: *RSC Adv.*, 2017, **7**, 19604

# Near infrared laser-controlled drug release of thermoresponsive microgel encapsulated with $Fe_3O_4$ nanoparticles

Xiaofang Qi,[ab] Lu Xiong,[b] Jing Peng[b] and Dongyan Tang *[ab]

Received 23rd January 2017
Accepted 18th March 2017

DOI: 10.1039/c7ra01009e

rsc.li/rsc-advances

One major issue in thermosensitive drug delivery systems is the remote, repeatable control of temperature *in vivo* through external stimuli such as light, ultrasound, and magnetic field. In this study, an $Fe_3O_4$/p(NIPAM-*co*-MAA) composite microgel (Nms) was fabricated *via* copolymerizing NIPAM with MAA in water-containing $Fe_3O_4$ nanoparticles modified by oleic acid. The photothermal effect and thermal-responsibility of Nms were investigated by adjusting the amount of MAA and $Fe_3O_4$ in the reaction, and the result shows an LCST of 37.2 °C, which could be elevated to 45.8 °C under laser treatment at 808 nm. In the drug release experiment, the data show that the drug can be released at an expected rate by controlling the temperature using an 808 nm laser irradiation *in vivo*. The release rate was fast and the final cumulative drug release rate increased by about 25%. Thus, these properties of the $Fe_3O_4$/p(NIPAM-*co*-MAA) Nms microgel indicate its promising application in multi-responsive microgels, especially in photothermal drug carriers.



## 1. Introduction

Stimuli-responsive microgels have been well-studied and widely applied in many fields such as tissue engineering, biomedical implants,[1] drug delivery,[2] and bionanotechnology,[3] owing to their three-dimensional (3D) physical structure,[4] good mechanical properties,[5] and high water content.[6] Especially, thermal-responsive microgels based on poly(*N*-isopropylacrylamide) (PNIPAM) exhibit a lower critical solution temperature (LCST) at about 32 °C,[7] which is approximate to the physiological temperature of the human body.[8] Moreover, when the surrounding temperature increases, polymeric microgels undergo a phase transformation from a swollen structure to collapse aggregation,[9] which provides an opportunity to load and/or release small molecules and thus potential application in cancer therapy.

However, once heated, PNIPAM microgels collapse from the swollen gel in an uncontrollable way, which limits its application in drug-controlled release. Some other stimuli such as pH (AAc),[10] oxidoreduction (GSH),[11] and near-infrared (NIR) light (CuS)[12] were introduced to adjust the drug release rate. Among all these strategies, NIR absorbing materials can be used as a photothermal ablation agency by transforming light into thermal energy[13] to kill cancer cells or release drugs.[14] NIR photothermal semiconductor nanocystals such as $MoS_2$,[13] $WS_2$,[15] and $Cu_9S_5$ (ref. 16) have become popular because they are inexpensive and readily available. However, some researchers have reported that the potential toxicity,[17] undegradability,[18] and low hemolytic activity[16] impair their application in biomedicine to some extent. Although $Fe_3O_4$ nanoparticles could avoid these problems and effectively absorb NIR light, and have been clinically applied in hyperthermia cancer therapy using NIR,[19] poor dispersion stability and easy aggregation usually lead to low activity of $Fe_3O_4$ nanoparticles.[10] One way to overcome these disadvantages is to put them in a polymeric microgel for the stabilization of $Fe_3O_4$ nanoparticles. Moreover, the composite microgel would not only exhibit stronger NIR light absorption but also achieve excellent controlled drug release by adjusting the NIR irradiation power.

Additionally, some similar systems including Au@$SiO_2$/P(NIPAM-*co*-AAc),[14] PANI/PNIPAM/HPC,[11] and rNGO@m$SiO_2$@-pNIPAM-*co*-pAAm[12] have been reported. Inspired by these composite systems and the related assembly methods, we prepared an $Fe_3O_4$/p(NIPAM-*co*-MAA) microgel by compositing a layer of PNIPAM on the surface of $Fe_3O_4$ nanoparticles. As shown in Fig. 1, we first synthesized $Fe_3O_4$ nanoparticles modified with oleic acid. After this, the nanoparticles were copolymerized with NIPAM and MAA monomers *via* polymerization in an emulsion. Finally, the photothermal effect and thermal-responsibility of $Fe_3O_4$/p(NIPAM-*co*-MAA) were investigated by determining its drug control release capacity under 808 nm laser irradiation. The irradiation results indicate that the composite microgel could increase the temperature from 30 to 45.8 °C and the cumulative drug released amount increased by

[a]*State Key Laboratory of Urban Water Resource and Environment, Harbin Institute of Technology, Harbin 150090, China. E-mail: xiaofangqixiao@163.com; dytang@hit.edu.cn*

[b]*School of Chemistry and Chemical Engineering, Harbin Institute of Technology, Harbin 150001, China*

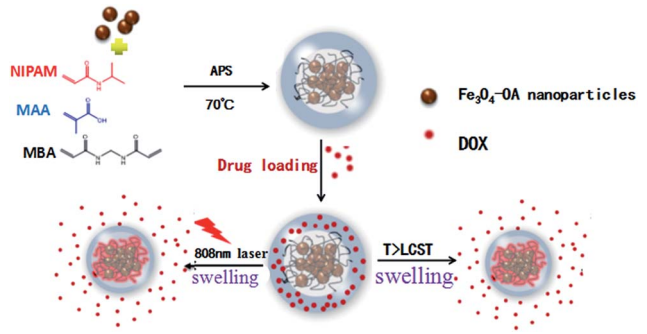


Fig. 1 Schematic for the preparation process and NIR light-triggered drug release of $Fe_3O_4$/p(NIPAM-*co*-MAA) Nms.

about 25%. The results suggest that the composite microgel Nms exhibits great advantages for photothermal/chemotherapy.[19]

## 2. Experimental

### 2.1 Materials

Ferric chloride hexahydrate ($FeCl_3 \cdot 6H_2O$), ferrous chloride tetrahydrate ($FeCl_2 \cdot 4H_2O$), ammonia water ($NH_3 \cdot H_2O$), oleic acid (OA), doxorubicin (DOX), absolute ethyl alcohol, sodium hydrogen phosphate ($Na_2HPO_4$), sodium chloride (NaCl), and isopropyl alcohol were purchased from Xilong Chemical Co., Ltd (Guangdong, China) and used without any further purification. *N*-isopropylacrylamide (NIPAM), methacrylic acid (MAA), ammonium persulfate (APS), *N*,*N*-methylene bisacrylamide (MBA), and sodium dodecyl sulphate (SDS) were all analytically pure and were purchased from Aladdin Co., Ltd.

### 2.2 Synthesis of OA-modified $Fe_3O_4$ nanoparticles

$Fe_3O_4$ nanoparticles were synthesized by the co-precipitation of iron chloride salts with ammonia.[19] In a typical synthesis process,[20,21] 4.43 g $FeCl_3 \cdot 6H_2O$ and 1.625 g $FeCl_2 \cdot 4H_2O$ were dissolved in 190 mL deionized water under mechanical stirring at 60 °C under a nitrogen atmosphere. Under the conditions of vigorous stirring, 10 mL $NH_3 \cdot H_2O$ was poured into the above-mentioned solution. After stirring for 30 min, the solution was precipitated by centrifugation and black precipitates obtained were washed three times with ethanol and water. Then, the $Fe_3O_4$ nanoparticles were redispersed in 180 mL deionized water and heated to 60 °C under the protection of nitrogen gas, and mixture solutions of 0.9 g oleic acid and 3 mL ammonia water were added within 30 min. After this, the solution was heated at 80 °C and precipitation occurred. The precipitate was washed with acetone 3 times and then dried in a vacuum oven at 70 °C for 24 h. The $Fe_3O_4$ nanoparticles modified by oleic acid were labelled as OA–$Fe_3O_4$.

### 2.3 Fabrication of p(NIPAM-*co*-MAA) with OA-modified $Fe_3O_4$ nanoparticles

The $Fe_3O_4$/p(NIPAM-*co*-MAA) composite microgel was synthesized *via* a emulsion polymerization method, as previously described.[22] Herein, 0.5 mg of OA–$Fe_3O_4$ nanoparticles was mixed with 15 mL sodium dodecyl sulfate (SDS, 1.0 mg $mL^{-1}$) containing 300 mg *N*-isopropylacrylamide (NIPAM, monomer), 15 μL methacrylic acid (MAA, monomer), and 10 mg bisacrylamide (MBA, cross-linker). This mixture was vigorously stirred and ultrasonicated, and a brown emulsion was obtained. This mixture was then heated to 70 °C and bubbled with nitrogen to remove the residual oxygen. Thereafter, 1.0 mL (10 mg $mL^{-1}$) ammonium persulfate (APS), as an initiator, was rapidly added, and polymerization was allowed to proceed at 70 °C for 6 h. Finally, the obtained $Fe_3O_4$/p(NIPAM-*co*-MAA) composite microgel was further purified (Spectra/Por molecular porous membrane tubing, cut-off 12 000–14 000 Da), dialyzed for four weeks against very frequently changing water at room temperature (25 °C), and then dried under vacuum at 50 °C. This $Fe_3O_4$/p(NIPAM-*co*-MAA) nanocomposite was labeled as Nms.

### 2.4 DOX loading and controlled release from $Fe_3O_4$/p(NIPAM-*co*-MAA)

The composite microgel (24 mg) was dispersed in 10 mL deionized water. The resulting composite microgel solution was poured into a dialysis bag (cut-off molecular weight of 8000–14 000 Da), the dialysis bag was placed in a 50.0 mL solution containing the anticancer drug DOX, and then left at room temperature for 24 h. A UV-spectrophotometer was used to measure the transmittance of the dialysate at 480 nm and to obtain the loading amount according to the DOX standard curve. Moreover, the products were cleaned using deionized water, which was repeated at least five times until a colorless supernatant was obtained.

For photothermal-triggered release, according to Huang's method,[22] 1.0 mL PBS (pH = 7.4) containing Nms@DOX (1.0 mg $mL^{-1}$) in a 10 mL test tube was incubated at 37 °C. At predetermined time intervals, the samples were irradiated using an 808 nm NIR laser with an output power density of 1.0 W $cm^{-2}$ for a certain period of time. The samples were centrifuged (8000 rpm, 10 min) and DOX was quantified *via* UV-spectrophotometer analysis using the supernatants. Finally, fresh PBS (5 mL) was added to the residual mixture.

### 2.5 Characterization

FTIR spectra were obtained at room temperature by a spectrometer (AVATAR 360, Nicolet, USA) and measured in the wavenumber range from 4000 to 400 $cm^{-1}$ by dispersion in KBr matrices to elucidate the key structural features. The surface of the composite microgel was observed using a field emission electron microscope (SEM) (Helios Nanolab 600i, FEI, USA) after coating with gold.[23] Transmission electron microscopy (TEM, JEOL, Japan) images were acquired using a JEOL JEM-1400 TEM operating at the acceleration voltage of 120 kV. The thermoresponsive behavior of the composite microgel was investigated using the transmittance of a temperature-controlled UV-spectrophotometer (TU-1901, Purkinje, China). Drug release data were monitored using a UV-spectrometer at the wavelength of 480 nm. The light scattering (DLS) size of Nms was measured

using Zetasizer Nano (Enigma Business Park, Grovewood Road, Malvern, Worcestershire. WR141XZ, United Kingdom). The structures of OA–$Fe_3O_4$ nanoparticles were identified by XRD (Bruker D8, Bruker AXS, Germany).

# 3. Results and discussion

## 3.1 Morphology and structures

The transmission electron microscopy (TEM) images depicted in Fig. 2a and b show that the size of the OA–$Fe_3O_4$ sample is about 10 nm. Clearly, most of the $Fe_3O_4$ nanoparticles are coated with OA. The higher magnification TEM image (Fig. 2c) reveals that the lattice spacing is 0.253 nm, which is consistent with the *d* value of the (311) planes of $Fe_3O_4$. In Fig. 2d, the SEM image of the composite microgel Nms-MAA-20, prepared with a MAA comonomer amount of 20 μL, shows that the sample is a spherical microgel with a diameter of about 400 nm. To further investigate whether $Fe_3O_4$ nanoparticles were successfully coated with the thermosensitive polymer, the composite microgel was observed *via* TEM (Fig. 2e and f). It was found that the composite microgel had agglomerations with a diameter of about 400 nm, in which the black center denotes the OA–$Fe_3O_4$ core, whereas the gray layer around the center is the copolymer shell. During the reaction, the existence of electrostatic repulsion between oleic acid and $COO^-$ led to unsatisfactory coating of the microgel on the OA–$Fe_3O_4$ nanoparticles. Through ultrasonication, this situation was obviously improved. As shown in Fig. 2f, $Fe_3O_4$ nanoparticles are encapsulated into microgel with the overall size of about 180 nm and the thickness of about 80 nm. Therefore, we conclude that the $Fe_3O_4$ nanoparticles were successfully coated with the temperature-responsive polymer.

The samples with different amounts of $Fe_3O_4$ nanoparticles (0.5 mg and 5 mg) are displayed in Fig. 2e and f, respectively, in which obvious differences can be observed. However, it was found that the $Fe_3O_4$ fraction around the composite microgel (Fig. 2f) is relative in the sample with less $Fe_3O_4$ nanoparticles. This suggests that only a few monomers were involved in the polymerization reaction, such that a lower content of $Fe_3O_4$ nanoparticles was in the microgel and the 5 mg $Fe_3O_4$ sample reached saturation within the reaction system solution. To further increase the content of $Fe_3O_4$ nanoparticles, the electrostatic interaction between inorganic nanoparticles and polymer microgel could be used in the process of the ultrasound irradiation method[25] since the prepared OA–$Fe_3O_4$, initiator APS, and comonomer are charged. Thus, the second capsulation could improve the amount of $Fe_3O_4$ nanoparticles in the composite microgel by ultrasound treatment. As shown in Fig. 3a and b, the composite microgel containing 0.5 mg of $Fe_3O_4$ nanoparticles was observed by SEM before and after the second capsulation. The results indicate that they have a similar morphology; however, we were unable to determine whether the $Fe_3O_4$ nanoparticles were absorbed into the composite microgel. By investigating the photothermal efficiency of the second capsulation composite microgel, it was observed that the temperature of the composite microgel after the second capsulation exhibited a pronounced increase under an 808 nm laser irradiation, and the highest elevated temperature was about 42 °C, which is higher than that in the previous capsulation.

## 3.2 Characterization of $Fe_3O_4$ and OA–$Fe_3O_4$ nanoparticles

**3.2.1 VSM.** The magnetic properties of the OA–$Fe_3O_4$ nanoparticles were investigated using a SQUID magnetometer. The $Fe_3O_4$ and OA–$Fe_3O_4$ hysteresis loops and magnetic optical images are depicted in Fig. 4. This sample exhibited the superparamagnetic behavior of $Fe_3O_4$ (Ms = 70 emu $g^{-1}$) and OA–$Fe_3O_4$ (Ms = 60 emu $g^{-1}$) due to its near zero coercivity and remanence, which indicate that OA–$Fe_3O_4$ does not change the magnetism compared with $Fe_3O_4$, and these nanoparticles would be an important candidate for biomedical applications.

**3.2.2 XRD.** To further ensure the structure of the OA–$Fe_3O_4$ nanoparticles, its XRD patterns (Fig. 5) were obtained and they matched well with the XRD patterns of the standard spinel type of $Fe_3O_4$ (JCPDS card file no: 19-0629).[2] The characteristic peaks of $Fe_3O_4$ crystals marked by their indices (220), (311), (400), (422), (440), and (533) can be observed in the patterns of the samples. Compared with $Fe_3O_4$, the peak intensity of OA–$Fe_3O_4$ remains unchanged, suggesting that the diffraction peaks of the two samples are identical. Furthermore, the result shows that the diffraction peaks of the two samples are all certainly

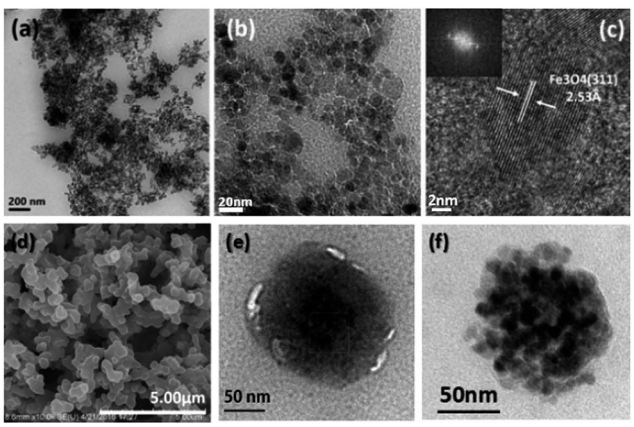


Fig. 2 (a)–(c) TEM images of OA–$Fe_3O_4$, (d) SEM images of Nms, and (e) and (f) TEM images of Nms with 0.5 mg and 5 mg OA–$Fe_3O_4$ nanoparticles, respectively.

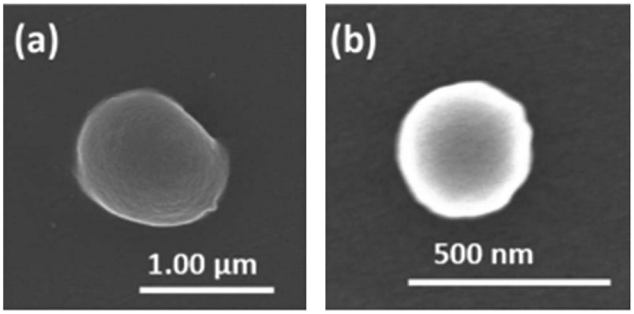


Fig. 3 SEM of Nms (a) before and (b) after the second capsulation.

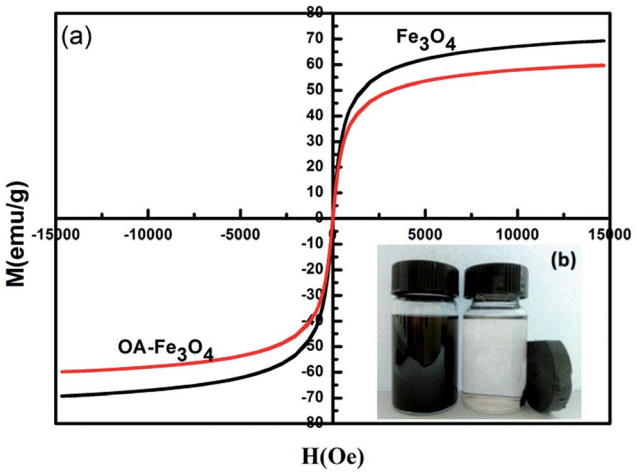


Fig. 4 (a) Magnetic hysteresis loops of OA–$Fe_3O_4$ and $Fe_3O_4$ and (b) magnetic optical image of OA–$Fe_3O_4$ and $Fe_3O_4$ nanoparticles.

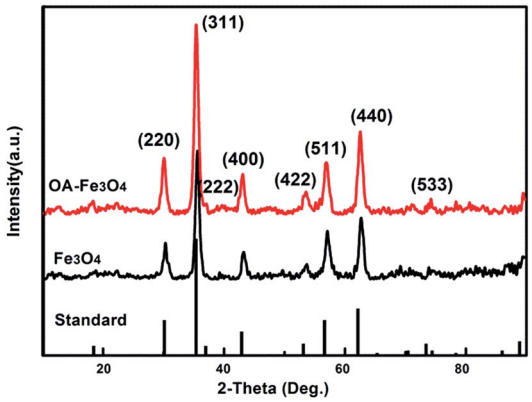


Fig. 5 XRD patterns of OA–$Fe_3O_4$ and $Fe_3O_4$ nanoparticles.

broadened, and the prepared nanoparticles are smaller in size. However, the average particle sizes are corrected from those obtained *via* TEM as approximately 127 nm as a result of the higher crystallinity of the prepared OA–$Fe_3O_4$ nanoparticles.

### 3.3 Characterization of $Fe_3O_4$/p(NIPAM-*co*-MAA)

The structures of the as-obtained composite microgel Nms and p(NIPAM-*co*-MAA) microgel were further characterized by Fourier transform infrared (FTIR) spectroscopy (Fig. 6a). The peak at 570 $cm^{-1}$ is characteristic of the stretching vibrations of Fe–O. The absorption bands at 2976, 2937, and 2877 $cm^{-1}$ correspond to the symmetric and asymmetric stretching vibrations of $-CH_3$ and $-CH_2$, respectively. In the infrared spectrum of OA–$Fe_3O_4$, it can be observed that $COO^-$ was chemically adsorbed on the surface of $Fe_3O_4$, and the stretching vibration peak was shifted to 1631 $cm^{-1}$ due to the coupling of $Fe^{3+}$. Compared with the p(NIPAM-*co*-MAA) and Nms curves, the peaks at 369 $cm^{-1}$ and 1386 $cm^{-1}$ are the bending vibrations of $-C(CH_3)_2$, 1637 $cm^{-1}$ and 1548 $cm^{-1}$ are the characteristic absorption peaks of amide I and amide II, respectively, and the broad absorption peak near 3478 $cm^{-1}$ occurred due to the overlapping of –OH and *N*–H bonds. Specifically, the dynamic light scattering (DLS) size of the Nms prepared with 20 μL MAA was 318.3 nm at 25 °C (Fig. 6b), which is comparable to that reported in earlier studies,[24] and good dispersion could be observed from the figure without larger or smaller particles. Underwent reversible shrinks and swells, well cycles of these Nms by switching the temperature between 25 °C and 50 °C (Fig. 6c) were achieved, suggesting their applicability in long-term stable thermosensitive drug release. To adjust its response to temperature and pH in cancer-tumor, the hydrophilic and acidic monomer MAA was introduced into the PNIPAM-based microgel. Fig. 6d depicts the LCST measured using a turbidity curve, which shows that the LCST of Nms with the comonomer MAA amounts of 10 μL, 20 μL, and 30 μL was 35.4 °C, 37.2 °C, and 38.3 °C, respectively. The LCST of the composite microgel with MAA was higher than that of pure PNIPAM (which was about 32 °C). This result indicates that the MAA monomer could increase the LCST of the composite microgel. TG measurement could roughly determine the content of $Fe_3O_4$ nanoparticles in the synthesized microgel. The TG/DTG curves of Nms are shown in Fig. 6e. The DTG derivative curves from room temperature to 690.8 °C show two distinct transitions for the composite microgel, and the TG curves indicate three weight loss processes (Nms lost ~2% residual water from room temperature to 307.5 °C; ~93.8% due to the decomposition of organic components from 310.5 °C to 502.6 °C, which suggests the existence of a small amount of $Fe_3O_4$ nanoparticles; and no remarkable weight loss in the range of 502.6–700 °C, which suggests the remaining $Fe_3O_4$ nanoparticles of about 0.36%)

### 3.4 Photothermal conversion of OA–$Fe_3O_4$ and $Fe_3O_4$/p(NIPAM-*co*-MAA)

The OA–$Fe_3O_4$ nanoparticles within an aqueous suspension show a broad and continuous absorption spectrum[19] and the NIR absorption intensity increased with the concentration of OA–$Fe_3O_4$ nanoparticles (Fig. 7a). The photothermal conversion effect was also initially studied on dry OA–$Fe_3O_4$ nanoparticle powders, which were exposed to an 808 nm laser irradiation at a relatively low power density (1 W $cm^{-2}$) (Fig. 7b). The heating curves of these solutions were similar to those of OA–$Fe_3O_4$ nanoparticles and showed rapid heating and large temperature increments depending on the concentrations. The photothermal effects of the $Fe_3O_4$/p(NIPAM-*co*-MAA) Nms solution with different amounts of OA–$Fe_3O_4$ nanoparticles at 0.5, 3.0, and 5.0 mg were exposed to an 808 nm NIR laser irradiation at the power density of 1.0 W $cm^{-2}$ for 5 min (Fig. 8). In contrast to water, Nms showed a concentration-dependent temperature increase. We also clearly observed similar temperature increase processes of Nms at different points of times, which could be directly attributed to the efficient absorption of the 808 nm NIR laser irradiation by Nms. The photothermal conversion efficiency could reach up to ~30%. After this, the photothermal efficiency of the composite microgel after second capsulation was found to increase under the 808 nm laser irradiation (Fig. 9a), and the highest elevated temperature was about 42 °C, which is higher than that in the previous capsulation. Moreover, the composite microgels with 0.5 mg and 5.0 mg $Fe_3O_4$

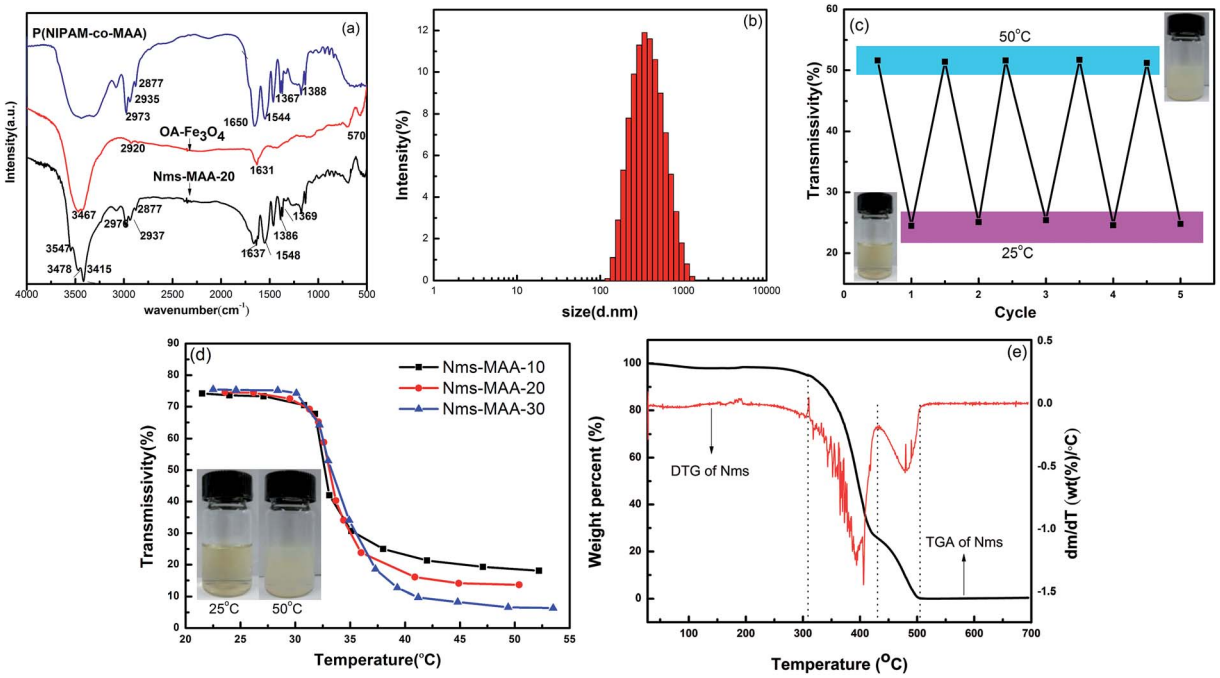


Fig. 6 (a) FT-IR spectra of p(NIPAM-*co*-MAA), OA–$Fe_3O_4$, and Nms, (b) DLS size and distribution of Nms, (c) transmissivity change of Nms by switching the temperature between 25 and 50 °C, (d) LCST of Nms by testing the change in transmissivity with temperature, and (e) TGA and DTG of Nms.

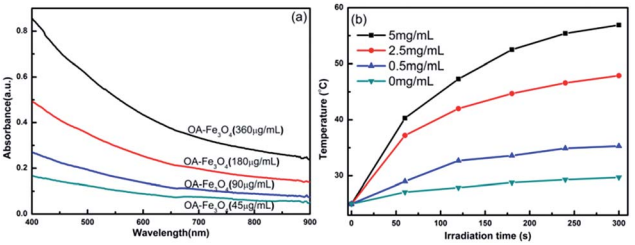


Fig. 7 (a) UV-vis absorption spectra of OA–$Fe_3O_4$ nanoparticles at different concentrations and (b) temperature evaluation of OA–$Fe_3O_4$ nanoparticles at different concentrations under 808 nm laser irradiation for 5 min.

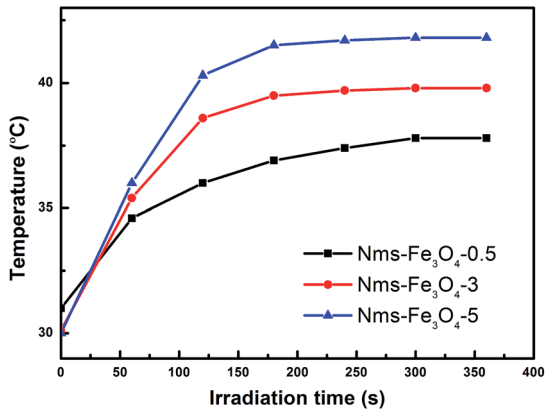


Fig. 8 Temperature evaluation of Nms with different amounts of OA–$Fe_3O_4$ under an 808 nm laser irradiation for 5 min.

nanoparticles, obtained through second capsulation, were irradiated under the 808 nm laser irradiation (Fig. 9b). The composite microgel with 5.0 mg $Fe_3O_4$ nanoparticles obtained through second capsulation had significantly higher photothermal efficiency as compared to the former, and the temperature could reach up to 45.8 °C within 5 min under an irradiation power density of 1.0 W $cm^{-2}$. Therefore, all our outcomes reveal that the optimized $Fe_3O_4$/p(NIPAM-*co*-MAA) Nms displays excellent photothermal conversion efficiency, which is favorable for controlled photo-thermosensitive drug release.

### 3.5 NIR photothermally controlled drug release

Encouraged by the excellent photothermal properties of Nms, DOX (a drug model) was loaded into Nms *via* electrostatic interaction and hydrogen bonds. The quantitative analysis of DOX as a result of drug release was studied using different concentrations of DOX standard solutions, and the transmittance of a UV-vis spectrophotometer was used at the wavenumber of 480 nm. The different concentrations of DOX in aqueous solutions following the Lambert–Beer law are presented in Fig. 10a, and the $R^2$ value of the fitted curve is 0.997. Then, the cumulative release rate was investigated. Details of the analysis include incubation of the DOX-loaded composite microgels in a PBS solution at pH 7.4 and keeping the samples at 30 °C for 1 h before the release. The DOX concentration was measured every 30 min and the 808 nm laser irradiation was turned on and the samples were irradiated at the power density of 1.0 W $cm^{-2}$. The sample was analyzed after 10 minutes, and the abovementioned steps were repeated until the DOX concentration was not

 

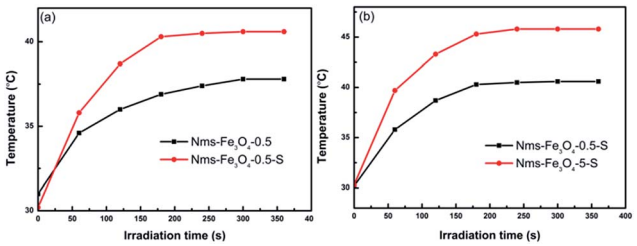


Fig. 9 (a) Temperature evaluation of Nms at an OA–$Fe_3O_4$ content of 0.5 mg before and after the second capsulation under an 808 nm laser irradiation for 5 min and (b) temperature evaluation of Nms with different amounts of OA–$Fe_3O_4$ under an 808 nm laser irradiation for 5 min by second capsulation.

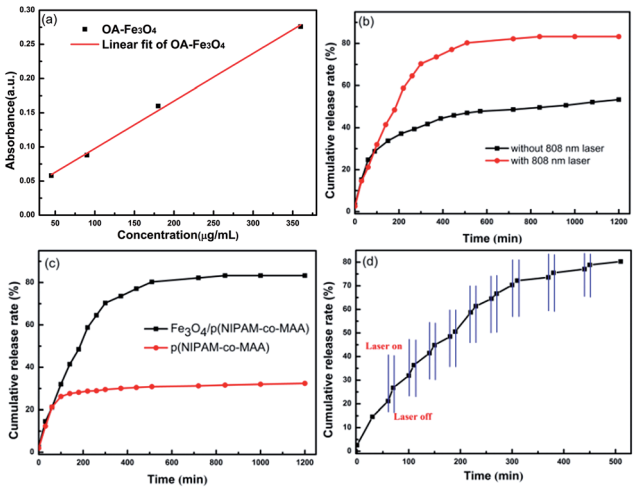


Fig. 10 (a) Standard curve of DOX, (b) DOX cumulative release with time under dark conditions and an 808 nm laser irradiation, (c) DOX cumulative release of p(NIPAM-*co*-MAA) and $Fe_3O_4$/p(NIPAM-*co*-MAA) with time under an 808 nm laser irradiation, and (d) DOX cumulative release with time by on/off 808 nm laser irradiation.

significantly increased. The cumulative release rate formula (equation) could be represented as follows:

$$\text{cumulative release rate} = \frac{v_1 \times c_i + v_2 \sum c_{(i-1)}}{m} \times 100\%$$

where $v_1$ is the total volume of the PBS solution (200 mL), $c_i$ is the concentration of the drug in the PBS solution, $v_2$ is the volume of the sample (3 mL), and $m$ is the total quality of the composite microgel. The calculated total amount of DOX loading within 24 mg composite microgel was 3.7 mg. As shown in Fig. 10b, the slow drug release of the composite microgels at 30 °C was investigated under dark conditions and an 808 nm laser irradiation. The cumulative release rate of the drug-loaded microgel under an 808 nm laser irradiation is faster than that without laser irradiation. The two curves indicate that DOX was quickly released in the first 5 h, then gradually released, and finally there was no obvious drug release after 16 h (within the PBS solution at the pH value of 7.4). The drug release of the composite microgel was tested under an 808 nm laser, as shown in Fig. 10b and c. The composite microgel containing $Fe_3O_4$ nanoparticles without the irradiation of the 808 nm laser only released about 40% of the drug, which is far lower than that by the composite microgel irradiated with the 808 nm laser (Fig. 10b). In the $Fe_3O_4$/p(NIPAM-*co*-MAA) microgel, $Fe_3O_4$ nanoparticles works as the photothermal agent and could transform light into thermal energy to increase the temperature of the composite microgel upon laser irradiation. However, the microgel without $Fe_3O_4$ nanoparticles could not be affected and changed by 808 nm laser irradiation, and thus the tiny release amount of drug, as shown in Fig. 10c, is mostly induced from the diffusion effect of the laser. As shown in Fig. 10d, the cumulative release curve of the drug indicates that the drug release rate under the 808 nm laser irradiation is extremely faster than that in the absence of the laser. Moreover, the final cumulative release rate was about 25%, which is higher than the cumulative release rate without 808 nm laser irradiation. Thus, we conclude that the prepared composite microgel could absorb NIR light and convert it into heat energy, and the promotion of the drug loaded and released rate are significantly increased under laser irradiation. The increase in the final cumulative release rate originated from the repeated heating and dropping of the composite microgel structure under intermittent 808 nm laser irradiation, which led to the composite microgel shrinking and swelling, respectively. The high cumulative release rate originated from the shrinking and swelling process of the microgel, which were driven by the intermittent irradiation of the NIR laser.

## 4. Conclusion

In summary, an $Fe_3O_4$/p(NIPAM-*co*-MAA) Nms composite microgel was prepared by the emulsion polymerization of NIPAM and MAA in the presence of OA–$Fe_3O_4$ nanoparticles. Nms exhibits both photothermal effects and thermo/PH field sensitivities, and its drug release rate could be increased by 25%. Further, after adjusting the amount of MAA, the LCST of the composite microgel could be increased to 37.2 °C and the temperature of Nms could be increased to 45.8 °C under an 808 nm laser irradiation by the second capsulation method. Due to its good biocompatibility and degradability, $Fe_3O_4$ nanoparticles show great promise in meeting the clinical requirements of mild irradiation and low dosage. Moreover, the magnetic properties of $Fe_3O_4$ nanoparticles could be used to separate proteins and enzymes as well as in nuclear magnetic resonance imaging.

## Acknowledgements

The authors are grateful for the Excellent Academic Leaders Foundation of Harbin, China (No. 2014RFXXJ017), and the Open Project of State Key Laboratory of Urban Water Resource and Environment, Harbin Institute of Technology (No. QA201610-02).

## References

1 S. S. Aravind, J. Costa, M. Pereira, V. Mugweru, A. Ramanujachary and T. D. Vaden, *Int. J. Hydrogen Energy*, 2014, **39**, 11528–11536.
2 H. Wu, G. P. Liu, Y. Zhuang, D. Wu, H. Zhang, H. Yang and S. Yang, *Biomaterials*, 2011, **32**, 4867–4876.
3 J. K. Oh, R. Drumright, D. J. Siegwart and P. Matyjaszewski, *Polym. Sci.*, 2008, **33**, 448–477.
4 A. S. Hoffman, *J. Controlled Release*, 1987, **6**, 297–305.
5 R. Langer and J. P. Vacanti, *Science*, 1993, **260**, 920–926.
6 R. Langer, *Science*, 2001, **293**, 58–59.
7 D. Crespy and R. M. Rossi, *Polym. Int.*, 2007, **56**, 1461–1468.
8 M. Ballauff and Y. Lu, *Polymer*, 2007, **48**, 1815–1823.
9 M. Quesada-Pérez, J. A. Maroto-Centeno, J. Forcada and R. Hidalgo-Alvarez, *Soft Matter*, 2011, **7**, 10536.
10 H. Kawaguchi, *Polym. Int.*, 2014, **63**, 925–932.
11 S. B. Abel, S. B. Abel, M. A. Molina, C. R. Rivarola, M. J. Kogan and Barbero, *Nanotechnology*, 2014, **25**, 495602.
12 H. Wan, Y. Zhang, Z. Liu, G. Xu, G. Huang, Y. Ji and H. zou, *Nanoscale*, 2014, **6**, 8743–8753.
13 S. S. Chou, B. Kaehr, J. Kim, B. M. Foley, M. De, P. E. Hopkins and V. P. Dravid, *Angew. Chem., Int. Ed.*, 2013, **52**, 4160–4170.
14 Z. Zhang, J. Wang, X. R. Nie, T. Wen, Y. Ji, X. Wu and R. Chen, *J. Am. Chem. Soc.*, 2014, 7317–7326.
15 G. S. Song, F. Jiang, R. Hu, W. P. Li and J. Hu, *ACS Appl. Mater. Interfaces*, 2014, **6**, 3915–3922.
16 Q. Tian, F. Z. Jiang, Q. Liu, Z. Chen, M. Zhu and J. Hu, *ACS Nano*, 2011, **5**, 9761–9771.
17 G. Song, Q. Wang, Y. Wang, G. N. Lv, R. Zou and J. Hu, *Adv. Funct. Mater.*, 2013, **23**, 4281–4292.
18 Q. Liu, C. Sun, Q. He, D. Liu, A. Khalil, T. Xiang and L. Song, *Chem. Commun.*, 2015, **51**, 10054–10057.
19 M. Chu, Y. Shao, J. Peng, X. Dai, H. Li, Q. Wu and D. Shi, *Biomaterials*, 2013, **34**, 4078–4088.
20 A. Bumb, M. W. Brechbiel, P. L. Choyke, L. Fugger and A. Eggeman, *Nanotechnology*, 2008, **19**, 335601.
21 J. Park, K. An, Y. H. Wang, J. G. Park, H. J. Noh, J. Y. Kim and T. Hyeon, *Nat. Mater.*, 2004, **3**, 891–895.
22 S. Huang, J. J. Liu, Q. He, H. C. Chen, S. Xu and L. Wang, *Nano Res.*, 2015, **8**, 4038–4047.
23 X. L. Lin, D. Y. Tang, Z. Q. Yu and Q. Feng, *J. Mater. Chem. B*, 2014, **2**, 651–658.
24 Y. S. Kang, S. Risbud, J. F. Rabolt and P. Stroeve, *Chem. Mater.*, 1996, **8**, 2209–2215.
25 J. Chen, C. Burger, C. V. Krishnan and B. J. Chu, *J. Am. Chem. Soc.*, 2005, **127**, 4140–4141.